Adaptive Constrained ICA with Mixing Matrix Column Constraints: Application to fMRI Data

Chunying Jia[1,*], Weixin Wang[1,*], Trung Vu[1], Hanlu Yang[1], Ben Gabrielson[1], Vince D. Calhoun[2], Tülay Adali[1]
Email: {chunyin1, wwang5, adali}@umbc.edu
[1]University of Maryland Baltimore County, Baltimore, MD 21250
[2]Tri-Institutional Center for Translational Research in Neuroimaging and Data Science (TReNDS),
Georgia State University, Georgia Institute of Technology, Emory University, Atlanta, GA 30303, USA

***Abstract*—Independent Component Analysis (ICA) is a powerful data-driven method that has been widely applied in functional magnetic resonance imaging (fMRI) data analysis to uncover underlying sources. An attractive way to boost ICA performance is via *constraints* to guide ICA factors to be similar to user-supplied "references", allowing incorporation of prior-knowledge into the factorization. However, most of existing constrained ICA methods typically only impose source constraints and are unable to impose constraints on the mixing matrix. With multi-subject medical imaging datasets, constraining the mixing matrix with subjects' symptom-related measurements, such as clinical scores or cognitive variables, enhances the algorithm's ability to identify brain activities associated with these symptoms. This offers a novel perspective for understanding the pathologies underlying various psychiatric disorders. Therefore, to overcome the limitations of existing constrained ICA algorithms, we introduce a new constrained ICA algorithm: adaptive-reverse constrained matrix entropy bound minimization (arc-M-EBM), which imposes constraints on the mixing matrix and uses adaptive-reverse thresholding to avoid overfitting or underfitting. This approach ensures flexibility and leads to more accurate and interpretable source separation. Simulations demonstrate that arc-M-EBM outperforms traditional ICA methods. Application to resting-state fMRI data from 176 subjects from healthy controls and patients reveals significant relationships between constrained components and clinical measures, enhancing our understanding of brain-behavior relationships.**

***Index Terms*— Constrained Independent Component Analysis, Adaptive Reverse Scheme, fMRI Analysis**

I. Introduction

Independent component analysis (ICA) is a powerful blind source separation technique used to uncover hidden sources from observed data [1], [2]. By assuming statistical independence and a linear mixing model, ICA extracts latent variables, i.e., sources, making it particularly useful for exploratory data analysis. Its data-driven nature has made ICA highly successful in analyzing functional Magnetic Resonance Imaging (fMRI) data. Incorporating constraints based on reliable prior information can significantly enhance the algorithm's separation performance when such data is available.

To address these limitations, constrained ICA (c-ICA) has been developed [3]. Constrained ICA can integrate prior knowledge, enhancing accuracy and interpretability. For example, by incorporating spatial constraints into fMRI data analysis, c-ICA provides clearer insights into brain activity [4], [5]. Subsequently, [6] proposed a framework that can extend the existing c-ICA for the mixing matrix and [7] by using an alternating scheme between constraints and demixing matrix, both using the Infomax algorithm. Among existing c-ICA methods, constrained Entropy Bound Minimization (c-EBM) has proven particularly successful. EBM offers a flexible approach to match source probability distributions and enables the decoupling of the demixing matrix without requiring an orthogonality constraint [8]. In multi-subject resting-state fMRI studies, c-EBM is shown to effectively identify subgroups and reveal meaningful brain networks with significant differences between them [9].

Despite its advantages, c-EBM lacks constraints on the mixing matrix, which limits its integration of critical prior knowledge such as cognitive or clinical measures. Applying such constraints could improve the contextual relevance and biological significance of the results. For example, linking symptom severity to the mixing coefficients of components facilitates the identification of symptom-specific components.

In this study, we develop adaptive-reverse constrained matrix EBM (arc-M-EBM) algorithm to address this limitation, which imposes constraints by encouraging the estimated mixing matrix columns to be similar to supplied *reference* columns, improving both separation performance and interpretability. The arc-M-EBM algorithm utilizes an adaptive thresholding strategy introduced by [10], dynamically adjusting constraint thresholds to prevent overfitting and underfitting. This ensures that the algorithm utilizes provided prior information without forcing the similarity between the estimated mixing matrix and the references to exceed a certain threshold. Furthermore, arc-M-EBM allows for the estimation of free components outside the provided references, offering flexibility while effectively capturing the underlying data structure. The flexibility in constraint selection and the inclusion of free components empower arc-M-EBM to effectively analyze complex neuroimaging datasets.

The application of arc-M-EBM to both simulated and real-world datasets has yielded promising results. In simulations, arc-M-EBM consistently outperforms traditional ICA techniques such as FastICA, Infomax, and EBM. When applied

*Chunying Jia and Weixin Wang contributed equally to this work.

**This work was supported in part by grants NSF 2316420, NIH R01MH118695, NIH R01MH123610, and NIH R01AG073949.

to real-world fMRI data, arc-M-EBM reveals significant associations between constrained components and clinical measures, highlighting its potential to uncover meaningful brain-behavior interactions. Specifically, the cerebellum component is associated with the Global Assessment of Functioning (GAF) score [11], while the parietal component correlates with the Montgomery-Åsberg Depression Rating Scale (MADRS) score [12]. The results align with previous studies, such as those reporting the cerebellum's role in schizophrenia and the associated cognitive impairment [13] and the involvement of parietal regions in depression pathophysiology [14]. These findings suggest that arc-M-EBM is a valuable tool for both theoretical and clinical applications, providing a robust framework for analyzing complex datasets.

II. Background

A. Independent Component Analysis

Consider N statistically independent, zero-mean, univariate latent sources $\mathbf{s} = [s_1, \ldots, s_N]^T$ and an unknown invertible mixing matrix $\mathbf{A} \in \mathbb{R}^{N\times N}$. ICA assumes a linear mixture model: $\mathbf{x} = \mathbf{As}$, where $\mathbf{x} \in \mathbb{R}^N$ is the observable mixture vector. Over V samples, the observed data matrix $\mathbf{X} \in \mathbb{R}^{N\times V}$ and the underlying sources $\mathbf{S} \in \mathbb{R}^{N\times V}$ are related by the equation $\mathbf{X} = \mathbf{AS}$.

The goal of ICA is to estimate a demixing matrix $\mathbf{W} = [\mathbf{w}_1, \ldots, \mathbf{w}_N]^T$ such that the estimated sources $\mathbf{y} = [y_1, \ldots, y_N]^T = \mathbf{Wx}$ are *maximally statistically independent*. Over the V samples, our estimated sources are given by $\mathbf{Y} = [\mathbf{y}_1, \ldots, \mathbf{y}_N]^T \in \mathbb{R}^{N\times V}$.

A natural strategy for maximizing source independence is minimizing their mutual information, expressed as a function of $\mathbf{W}$:

$$\mathcal{J}(\mathbf{W}) = \sum_{n=1}^{N} H(y_n) - \log|\det \mathbf{W}| - H(\mathbf{x}), \tag{1}$$

where $H(y_n) = -E[\log p_n(y_n)]$ represents the entropy of the nth source (estimated using its realization over V samples in $\mathbf{y}_n$), and the term $\log|\det \mathbf{W}|$ is as a regularization term that preserves volume across the directions of source estimation. Estimation of the entropy is crucial in the ICA algorithm.

EBM is an ICA algorithm that estimates entropy by bounding the entropy of the estimates using a numerical computational method [8]. The decoupling method introduced by [15] allows for more flexible and realistic modeling of source signals by relaxing the orthogonality constraint. This method enables each row of the demixing matrix $\mathbf{W}$ to be individually optimized, such that (1) can be expressed as a function of $\mathbf{w}_n$, the nth row of $\mathbf{W}$:

$$\mathcal{J}(\mathbf{w}_n) = \mathcal{H}(y_n) - \log|\mathbf{d}_n^T\mathbf{w}_n| + C, \tag{2}$$

where $||\mathbf{d}_n|| = 1$ and $\mathbf{d}_n$ is orthogonal to all rows of $\mathbf{W}$ except for $\mathbf{w}_n$, and C is a constant.

B. Constrained ICA

Given a reference $\mathbf{r}_n$ for the nth source $\mathbf{y}_n$, c-ICA can be formulated as:

$$\min_{\mathbf{w}_n} \mathcal{J}(\mathbf{w}_n) \quad s.t.\ \epsilon(\mathbf{y}_n, \mathbf{r}_n) \geq \rho_n, \tag{3}$$

where $\epsilon(\mathbf{y}_n, \mathbf{r}_n)$ represents a specific similarity measure between $\mathbf{y}_n$ and $\mathbf{r}_n$, defined as $\epsilon(\mathbf{y}_n, \mathbf{r}_n) = |\mathbf{y}_n^T\mathbf{r}_n|$. Let the constraint function $h_n(\mathbf{y}_n, \mathbf{r}_n) = \rho_n - \epsilon(\mathbf{y}_n, \mathbf{r}_n)$. The problem in (3) is a constrained optimization problem that can be solved using a Lagrangian framework [3], [6].

C. Adaptive Reverse Scheme

In c-ICA, the threshold parameters ρ_n are often unknown and need to be predetermined. If ρ_n values are set too high, the constraints become difficult to satisfy, leading to an unpredictable solution. Conversely, if ρ_n values are too low, the output may produce different components. To address this issue, [10] proposed an adaptive-reverse scheme to dynamically select variable thresholds for the constraints. The adaptive-reverse scheme adjust the values of ρ_n based on the similarity between the estimate $\mathbf{y}_n$ and the reference $\mathbf{r}_n$: when the similarity is insufficient, the algorithm reduces ρ_n; conversely, if the similarity is too high, the algorithm increases ρ_n. This dynamic adjustment helps maintain an optimal balance and improves the robustness of the solution.

III. Adaptive-Reverse Constrained Matrix EBM

In this study, we introduce arc-M-EBM, a novel method that imposes constraints on mixing matrix columns using an adaptive thresholding strategy. Given references $\mathbf{r}_n$ for rows of mixing matrix $\mathbf{w}_n$, we formulate the following constrained optimization problem:

$$\min_{\mathbf{w}_n} \mathcal{J}(\mathbf{w}_n) \quad s.t.\ \epsilon(\mathbf{r}_n, \mathbf{w}_n) \geq \rho_n, \tag{4}$$

where we assume that the columns of mixing matrices and references are unit norm and zero mean, $\epsilon(\mathbf{r}_n, \mathbf{w}_n) = |\mathbf{r}_n^T\mathbf{w}_n|$. Let $h_n(\mathbf{w}_n, \mathbf{r}_n) = \rho_n - \epsilon(\mathbf{w}_n, \mathbf{r}_n)$. Following the approach in [16], we address the problem in (4) using the augmented Lagrangian optimization function:

$$\mathcal{J}^c(\mathbf{w}_n, u_n) = \mathcal{J}(\mathbf{w}_n) + \frac{1}{2\gamma_n}((\max\{0, \gamma_n h_n(\mathbf{w}_n, \mathbf{r}_n) + u_n\})^2 - u_n^2), \tag{5}$$

where u_n is a Lagrangian multiplier, $\gamma_n > 0$ is a scalar penalty parameter. For $n = 1, \ldots, M$, where M is the number of constrained columns and $M \leq N$, we use the gradient method to derive the update rules for $\mathbf{w}_n$ and u_n:

$$\Delta\mathbf{w}_n = \frac{\partial\mathcal{J}^c(\mathbf{w}_n, u_n)}{\partial\mathbf{w}_n} \propto E(p_n(\mathbf{w}_n^T\mathbf{x})\mathbf{x}^T) + \frac{\mathbf{d}_n^T}{\mathbf{d}_n^T\mathbf{w}_n} + u_n \text{sign}(\mathbf{r}_n^T\mathbf{w}_n)\mathbf{r}_n, \tag{6}$$

$$\mathbf{w}_n \leftarrow \mathbf{w}_n - \eta\Delta\mathbf{w}_n, \tag{7}$$

$$u_n \leftarrow \max\{0, \gamma(\rho_n - \epsilon(\mathbf{w}_n, \mathbf{r}_n)) + u_n\}, \tag{8}$$

where η is the step size for each iteration.

Adaptive reverse scheme: According to (8), if we over estimate the similarity between $\mathbf{w}_n$ and $\mathbf{r}_n$ by choosing a large threshold ρ_n, the constraint $\rho_n - \epsilon(\mathbf{w}_n, \mathbf{r}_n)$ becomes difficult to satisfy. Consequently, the Lagrangian multiplier u_n will tend to infinity. Conversely, underestimating the similarity by choosing a small ρ_n causes u_n to decrease towards zero. The adaptive-reverse scheme introduces two strategies for dynamically adjusting the threshold value ρ_n based on the values of u_n in each iteration: (i) **overshooting the similarity**: Choose the smallest ρ_n that satisfies the constraint:

$$\rho_n = \text{argmin}\{\rho : \rho > \epsilon(\mathbf{r}_n, \mathbf{w}_n)\}, \tag{9}$$

and (ii) **undershooting the similarity**: Choose the largest ρ_n that satisfies the constraint:

$$\rho_n = \text{argmax}\{\rho : \rho \leq \epsilon(\mathbf{r}_n, \mathbf{w}_n)\}. \tag{10}$$

In each iteration, for a predefined maximum value $u_{\max}$, if $u_n \leq 0$, we apply the overshooting strategy; if $u_n \geq u_{\max}$, we apply the undershooting strategy.

While the cost function is based on $\mathbf{r}_n$ and $\mathbf{w}_n$, prior information about the mixing parameters typically pertains to a single column of the mixing matrix. To bridge this gap, it is necessary to transform the reference $\mathbf{p}_n$ for the column of the mixing matrix into the reference $\mathbf{r}_n$ for a row of the demixing matrix $\mathbf{w}_n$. This transformation can be achieved using principal component analysis (PCA). PCA is a commonly used technique for dimensionality reduction that decreases the number of variables in a dataset while preserving the most critical information. PCA reduces the dimensionality of the original mixing matrix $\tilde{\mathbf{X}} \in \mathbb{R}^{K \times N}$ by projecting it onto a lower-dimensional space using $\mathbf{Q} \in \mathbb{R}^{N_k \times K}$, where $K \gg N_k$. After applying PCA, the transformed reference $\mathbf{r}_n$ for the row of the demixing matrix can be computed as $\mathbf{r}_n = \mathbf{Q}\mathbf{p}_n$.

IV. Simulation Results

This section evaluates the performance of the proposed method compared with existing ICA algorithms on two subsets of the Labeled Faces in the Wild (LFW) dataset, using simulated constraints for each source. In each subset, face images are artificially mixed, and arc-M-EBM as well as four ICA algorithms are applied for their separation.

The first subset contains data with high correlations among sources, violating the independence assumption of sources and leading to suboptimal separation performance by most existing ICA methods. The second subset features low correlations among sources, where current ICA methods demonstrate improved performance. The study will illustrate how incorporating constraints on the mixing matrix $\mathbf{A}$ enhances the performance of the ICA algorithm.

The LFW dataset is a collection of face photographs designed for research in unconstrained face recognition [17]. It comprises 13,233 images of 5,749 individuals, detected and centered using the Viola-Jones face detector, and sourced from the web. This dataset was created and maintained by researchers at the University of Massachusetts, Amherst. Figures 1 and 2 display the selection of the two sets of sources along with their corresponding correlation matrices.

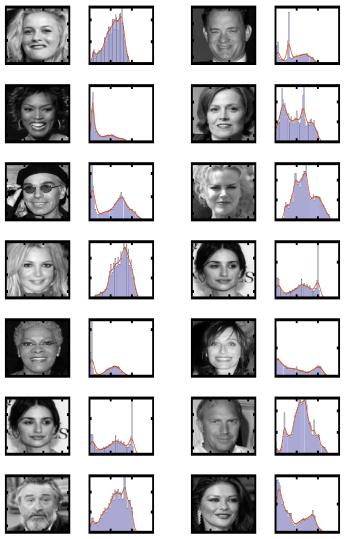

(a) (b)

Fig. 1: (a) Two sets of true sources from LWF with (a) low and (b) high correlation among sources. The histogram next to each image represents the distribution of the gray levels in that image.

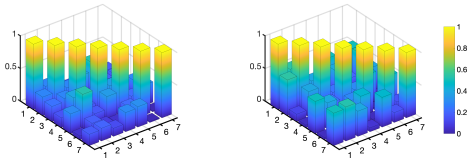

(a) (b)

Fig. 2: Cross-correlation values among face images for (a) the low-correlation source set; (b) the high-correlation source set.

Mixing matrix: Given the selected seven face images in each subset, let $\mathbf{S} \in \mathbb{R}^{7 \times P}$ represent the face sources, where P is the total number of pixels per image. The mixing matrix before dimension reduction, denoted as $\tilde{\mathbf{A}} \in \mathbb{R}^{K \times 7}$ with $K \gg 7$, is generated from a univariate Gaussian distribution for each entry. The mixture data $\tilde{\mathbf{X}} \in \mathbb{R}^{K \times P}$ is then created by $\tilde{\mathbf{X}} = \tilde{\mathbf{A}}\mathbf{S}$.

Constraint construction: After generating the original mixing matrix $\tilde{\mathbf{A}}$, we construct constraints for the sources using:

$$\tilde{\mathbf{r}}_i = \sqrt{1 - \alpha^2}\tilde{\mathbf{a}}_i + \alpha \mathbf{e}_i, \tag{11}$$

where $\tilde{\mathbf{a}}_i$ is the ith column of $\tilde{\mathbf{A}}$, and $\mathbf{e}_i \in \mathbb{R}^K$ is a vector with entries drawn from a normal distribution with zero mean and unit variance. The parameter α controls the noise level in the references $\tilde{\mathbf{r}}_i$. A larger α increases uncertainty about $\tilde{\mathbf{r}}_i$, reducing its quality.

Scenarios: We evaluate the performance of our proposed method, arc-M-EBM, under two distinct scenarios and com-

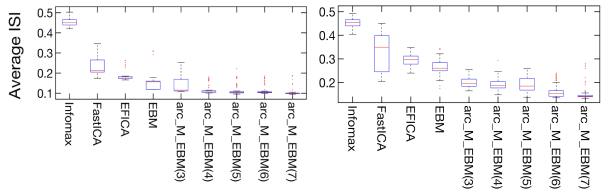

(a) (b)

Fig. 3: **Scenario 1**: ISI for different methods, including arc-M-EBM with fixed constraint uncertainty ($\alpha = 0.2$) and **varying numbers of constraints** for (a) the low-correlation source set and (b) the high-correlation source set. Numbers in parentheses after arc-M-EBM indicate the number of constraints used.

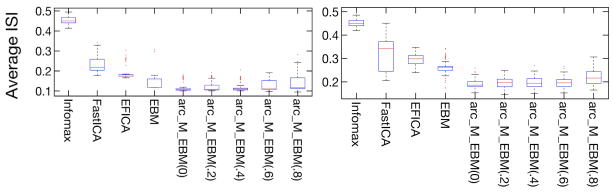

(a) (b)

Fig. 4: **Scenario 2**: ISI for different methods, including arc-M-EBM with fixed four constrained columns and **varying constraint uncertainty** (α) for (a) the low-correlation source set and (b) the high-correlation source set. Numbers in parentheses after arc-M-EBM indicate the uncertainty level (α).

pare it with four competing ICA methods: Infomax, FastICA, EFICA, and EBM.

Scenario 1: Varying number of constrained columns

We fix the uncertainty level $\alpha = 0.2$ and incrementally increase the number of constraints from three to seven for arc-M-EBM. This allows us to assess how the method's performance changes as more constraints are introduced.

Scenario 2: Varying uncertainty level

We fix the number of constrains to four and gradually increase the uncertainty level α from 0.2 to 0.8 for arc-M-EBM. This helps us understand the impact of varying uncertainty on the performance of arc-M-EBM.

Evaluation metric: To evaluate the performance of arc-M-EBM and other algorithms, we use the inter-symbol-interference (ISI) metric. ISI assesses how well the original independent components (ICs) are separated after the unmixing process. A lower ISI indicates nearly perfect separation, while a higher ISI suggests poorer performance [18].

Results for Scenario 1: Fig. 3 presents the ISI outcomes for Scenario 1, demonstrating the effects of incorporating prior information regarding the columns of the mixing matrix in both highly dependent and weakly dependent source datasets. With a fixed constraint noise level of $\alpha = 0.2$, the ISI decreases as the number of constrained columns increases. Notably, even with only three column references for the mixing matrix, arc-M-EBM consistently outperforms all competing ICA algorithms. This result highlights that integrating more prior information enhances the algorithm's ability to effectively separate the underlying latent sources.

Results for Scenario 2: Fig. 4 illustrates the simulation results under varying noise levels for a fixed number of constrained columns. The box plot shows that our method achieves the lowest ISI at low noise levels compare with unconstrained ICA algorithms. Moreover, arc-M-EBM continues to outperform most traditional ICA algorithms even when the noise level reaches approximately 60%. This demonstrates that incorporating references for the columns of the mixing matrix $\mathbf{A}$ significantly enhances the separation performance of ICA methods, even when the references are of lower quality. This robustness underscores the effectiveness of arc-M-EBM in challenging conditions.

Simulation results show that arc-M-EBM outperforms other ICA methods across various conditions. Even with nearly independent sources, incorporating reference information for the mixing matrix improves separation quality.

Traditional methods perform well at low source correlations but degrade as correlation increases. Arc-M-EBM, however, maintains strong performance in both low- and high-correlation scenarios. This robustness to deviations from the independence assumption highlights our approach's effectiveness and reliability in handling diverse levels of source dependence.

V. Application

A. fMRI Feature Dataset

The study used resting-state fMRI (rs-fMRI) datasets from the Bipolar and Schizophrenia Network for Intermediate Phenotypes (B-SNIP) project [19], [20], involving 176 patients with schizophrenia (SZs). For further details, see [21].

In this study, we used the max-TP feature, a recently proposed fMRI feature for capturing temporal peaks, which has shown promising results in differentiating between healthy controls and SZs. Max-TP features were calculated by averaging the 10 maximum values across all time points for each brain voxel [22]. A two-dimensional feature dataset was formed by concatenating the max-TP features across all subjects, resulting in a 176×40401 matrix, where rows correspond to subjects and columns to voxels.

B. Behavior Measures

Symptom ratings were collected using the Montgomery-Åsberg Depression Rating Scale (MADRS) [12] and the Global Assessment of Functioning (GAF) [11]. The MADRS assesses depressive symptom severity, with higher scores indicating more severe depression. The GAF rates social, occupational, and psychological functioning, with higher scores indicating better functioning.

Cognitive assessments were conducted using the Wide Range Achievement Test-IV (WRAT-IV) [23] and the Brief Assessment of Cognition in Schizophrenia (BACS) [24]. The WRAT-IV Spelling and Reading subtests (WRATSG) evaluate reading and math abilities, while the Token Motor Task

(BACS-Tok-Mot), a BACS subtest, measures motor speed and coordination.

In this study, MADRS, GAF, WRATSG, and BACS-Tok-Mot scores are utilized.

C. Implementation of arc-M-EBM

We applied arc-M-EBM to the max-TP feature dataset, using behavioral measures (MADRS, GAF, WRATSG, and BACS-Tok-Mot) as constraints on the mixing matrix columns. These constraints helped to integrate the subjects' clinical and cognitive profiles, assisting in identifying ICs whose mixing profiles are similar to these constraints. In our analysis, we constrained four columns of the mixing matrix while leaving the remaining columns unconstrained, allowing for a balanced approach between guided and exploratory data analysis.

To determine the suitable model order for arc-M-EBM, we used the cross-ISI metric [9], [25], [26]. Cross-ISI assesses component consistency across multiple runs, with smaller values indicating greater consistency and better model match. In contrast to ISI, cross-ISI does not rely on the true values of the mixing matrix $\mathbf{A}$, which enhances its practicality for real-world data analysis.

We determined model order through the following steps:

1) Conduct 30 runs of arc-M-EBM for each model order, ranging from 4 to 20 with a step size of 1, and then from 20 to 100 with a step size of 10;
2) Calculate the cross-ISI for all runs and visualize the distribution for each model order (Fig. 5);
3) Select model orders with small median values and low variance of cross-ISI.

Model order 12 exhibited the smallest median and relatively lower variance of cross-ISI (Fig. 5), making it the most appropriate choice. The final results were derived from the most consistent run with the smallest cross-ISI, using a model order of 12. The results remained consistent across different model orders.

D. Results

Fig. 6 displays the spatial maps of the constrained components and their correlations with behavioral measures for model order 12. IC1 is located in the cerebellum, IC2 in the parietal cortex, IC3 at the brain edges (likely representing motion artifacts), and IC4 within the ventricles (non-neural regions).

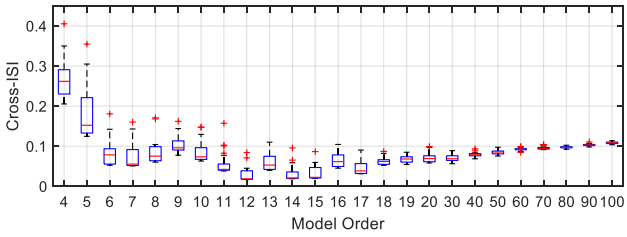

Fig. 5: Using cross-inter-symbol-interference (cross-ISI) to select a suitable model order for arc-M-EBM. The box plot shows the distribution of cross-ISI values for each model order. The median is represented by the central mark, and the bottom and top edges of the box indicate the 25th and 75th percentiles, respectively. Model order 12 exhibits the lowest median and relatively lower variance of cross-ISI values.

IC1 showed a significant correlation with the GAF score, aligning with the finding in [13], which highlighted the cerebellum's role in schizophrenia and associated cognitive impairment. IC2 correlated significantly with the MADRS score, consistent with the finding on the parietal cortex's involvement in depression reported in [14]. IC3 exhibited a significant correlation with WRATSG, while IC4, constrained to BACS-Tok-Mot, did not show a significant correlation.

Notably, meaningful ICs were significantly associated with symptom measures (MADRS and GAF) but not with cognitive measures (WRATSG and BACS-Tok-Mot). This distinction may be due to the nature of the measures. Symptom measures like MADRS and GAF are more directly related to the clinical presentation of schizophrenia, assessing the severity of depressive symptoms and overall functioning. Cognitive measures like WRATSG and BACS-Tok-Mot focus on specific cognitive functions and may not capture broader neural changes associated with the disorder.

VI. Conclusion

In this study, we introduced arc-M-EBM, a novel method that enhances ICA by incorporating prior knowledge into the mixing matrix with an adaptive-reverse thresholding strategy. Simulations demonstrate that when the constraints correspond to the true generative model, arc-M-EBM is able to significantly outperform other ICA-based methods, in terms of source separation and source *interpretability*: the sources' contextual meaning used to develop a greater understanding of the data. When applied to real-world fMRI data, arc-M-EBM revealed significant relationships between constrained components and clinical measures. These findings highlight the biological relevance and interpretability of the results, making arc-M-EBM a valuable tool for both theoretical exploration and clinical applications.

References

[1] P. Comon and C. Jutten. *Handbook of Blind Source Separation: Independent component analysis and applications*. Academic press, 2010.

[2] T. Adali, M. Anderson, and G.-S. Fu. Diversity in independent component and vector analyses: Identifiability, algorithms, and applications in medical imaging. *IEEE Signal Processing Magazine*, 31(3):18–33, 2014.

[3] W. Lu and J. Rajapakse. Constrained independent component analysis. *Advances in Neural Information Processing Systems*, 13, 2000.

[4] Q. Lin, J. Liu, Y. Zheng, H. Liang, and V. D. Calhoun. Semiblind spatial ICA of fMRI using spatial constraints. *Human Brain Mapping*, 31(7):1076–1088, 2010.

[5] H. Yang, F. Ghayem, B. Gabrielson, M. A. B. S. Akhonda, V. D. Calhoun, and T. Adali. Constrained independent component analysis based on entropy bound minimization for subgroup identification from multi-subject fMRI data. In *2023 ICASSP IEEE International Conference on Acoustics, Speech and Signal Processing (ICASSP)*, pages 1–5. IEEE, 2023.

[6] P. A. Rodriguez, M. Anderson, X. Li, and T. Adali. General non-orthogonal constrained ICA. *IEEE Transactions on Signal Processing*, 62(11):2778–2786, 2014.

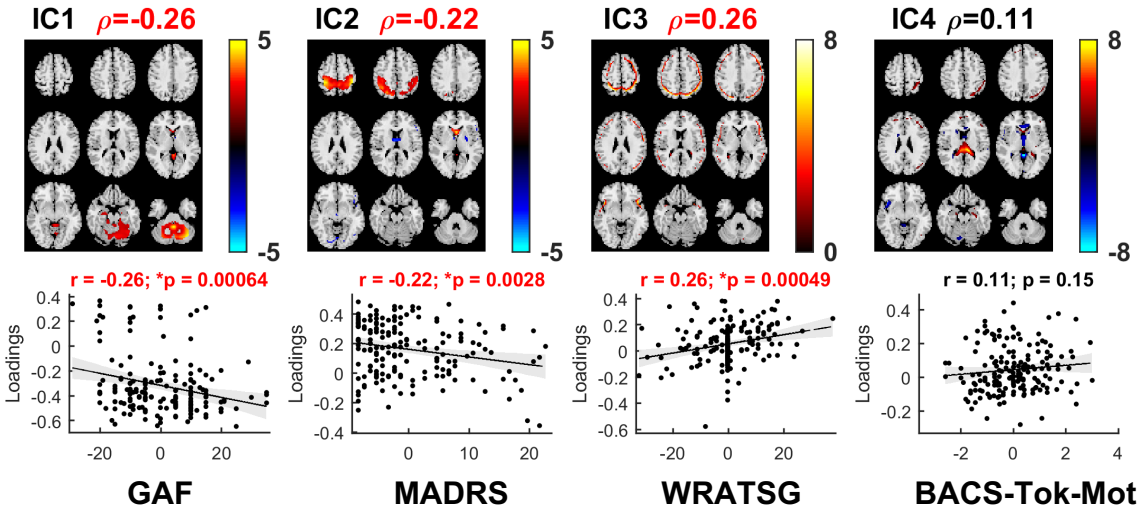

Fig. 6: Spatial maps and behavioral correlations. ICs associated with specific behavior scores are shown. Spatial maps of ICs were converted to Z-scores and thresholded ($|Z| \geq 2$). Pearson's correlation coefficients (ρ) above each map indicate the strength of correlations between subject loadings and behavior scores; significant coefficients ($p < 0.05$) are marked in red. Scatter plots illustrate the relationship between subject loadings and behavior scores, with Pearson's ρ and p-values shown above each plot. The solid line represents the best linear fit, and the shaded area indicates 95 % confidence interval. Black dots represent individual data points. Abbreviations: GAF: Global Assessment of Functioning; MADRS: Montgomery-Åsberg Depression Rating Scale; WRATSG: Wide Range Achievement Test-IV Spelling and Reading subtests; BACS-Tok-Mot: Brief Assessment of Cognition in Schizophrenia Token Motor Task.

[7] V. D. Calhoun, T. Adali, M. C. Stevens, K. A. Kiehl, and J. J. Pekar. Semi-blind ica of fmri: a method for utilizing hypothesis-derived time courses in a spatial ica analysis. *Neuroimage*, 25(2):527–538, 2005.

[8] X. Li and T. Adali. Independent component analysis by entropy bound minimization. *IEEE Transactions on Signal Processing*, 58(10):5151–5164, 2010.

[9] H. Yang, T. Vu, Q. Long, V. D. Calhoun, and T. Adali. Identification of homogeneous subgroups from resting-state fMRI data. *Sensors*, 23(6):3264, 2023.

[10] T. Vu, F. Laport, H. Yang, V. D. Calhoun, and T. Adali. Constrained independent vector analysis with reference for multi-subject fMRI analysis. *IEEE Transactions on Biomedical Engineering*, 2024.

[11] S. H. Jones, G. Thornicroft, M. Coffey, and G. Dunn. A brief mental health outcome scale: Reliability and validity of the Global Assessment of Functioning (GAF). *The British Journal of Psychiatry*, 166(5):654–659, 1995.

[12] S. A. Montgomery and M. Åsberg. A new depression scale designed to be sensitive to change. *The British Journal of Psychiatry*, 134(4):382–389, 1979.

[13] P. Faris, D. Pischedda, F. Palesi, and E. D'Angelo. New clues for the role of cerebellum in schizophrenia and the associated cognitive impairment. *Frontiers in Cellular Neuroscience*, 18:1386583, 2024.

[14] W. Liu, X. Jiang, Z. Deng, Y. Xie, Y. Guo, Y. Wu, Q. Sun, L. Kong, F. Wu, and Y. Tang. Functional and structural alterations in different durations of untreated illness in the frontal and parietal lobe in major depressive disorder. *European Archives of Psychiatry and Clinical Neuroscience*, 274(3):629–642, 2024.

[15] M. Anderson, X. Li, P. Rodriguez, and T. Adali. An effective decoupling method for matrix optimization and its application to the ICA problem. In *2012 IEEE International Conference on Acoustics, Speech and Signal Processing (ICASSP)*, pages 1885–1888. IEEE, 2012.

[16] W. Lu and Jagath C. R. Approach and applications of constrained ICA. *IEEE transactions on neural networks*, 16(1):203–212, 2005.

[17] G. B. Huang, M. Mattar, T. Berg, and E. Learned-Miller. Labeled faces in the wild: A database forstudying face recognition in unconstrained environments. In *Workshop on Faces in 'Real-Life' Images: Detection, Alignment, and Recognition*, 2008.

[18] S. Choi, A. Cichocki, L. Zhang, and S. Amari. Approximate maximum likelihood source separation using the natural gradient. *IEICE Transactions on Fundamentals of Electronics, Communications and Computer Sciences*, 86(1):198–205, 2003.

[19] C. A. Tamminga, E. I. Ivleva, M. S. Keshavan, G. D. Pearlson, B. A. Clementz, B. Witte, D. W. Morris, J. Bishop, G. K. Thaker, and J. A. Sweeney. Clinical phenotypes of psychosis in the bipolar-schizophrenia network on intermediate phenotypes (B-SNIP). *American Journal of psychiatry*, 170(11):1263–1274, 2013.

[20] S. A. Meda, G. Ruaño, A. Windemuth, K. O'Neil, C. Berwise, S. M. Dunn, L. E. Boccaccio, B. Narayanan, M. Kocherla, E. Sprooten, et al. Multivariate analysis reveals genetic associations of the resting default mode network in psychotic bipolar disorder and schizophrenia. *Proceedings of the National Academy of Sciences*, 111(19):E2066–E2075, 2014.

[21] Y. Du, G. D. Pearlson, D. Lin, J. Sui, J. Chen, M. Salman, C. A. Tamminga, E. I. Ivleva, J. A. Sweeney, M. S. Keshavan, et al. Identifying dynamic functional connectivity biomarkers using GIG-ICA: Application to schizophrenia, schizoaffective disorder, and psychotic bipolar disorder. *Human Brain Mapping*, 38(5):2683–2708, 2017.

[22] C. Jia, M. A. B. S. Akhonda, H. Yang, V. D. Calhoun, and T. Adali. Fusion of novel fMRI features using independent vector analysis for a multifaceted characterization of schizophrenia. In *2024 32nd European Signal Processing Conference (EUSIPCO)*, pages 1112–1116. IEEE, 2024.

[23] G. S. Wilkinson and G. J. Robertson. Wide range achievement test 4. *Journal of Clinical and Experimental Neuropsychology*, 1993.

[24] R. S. Keefe, T. E. Goldberg, P. D. Harvey, J. M. Gold, M. P. Poe, and L. Coughenour. The brief assessment of cognition in schizophrenia: reliability, sensitivity, and comparison with a standard neurocognitive battery. *Schizophrenia Research*, 68(2-3):283–297, 2004.

[25] Q. Long, C. Jia, Z. Boukouvalas, B. Gabrielson, D. Emge, and T. Adali. Consistent run selection for independent component analysis: application to fMRI analysis. In *2018 IEEE International Conference on Acoustics, Speech and Signal Processing (ICASSP)*, pages 2581–2585. IEEE, 2018.

[26] T. Adali, F. Kantar, M. A. B. S. Akhonda, S. Strother, V. D. Calhoun, and E. Acar. Reproducibility in matrix and tensor decompositions: Focus on model match, interpretability, and uniqueness. *IEEE Signal Processing Magazine*, 39(4):8–24, 2022.